Supporting Information

Regenerable and Stable Calix[4]pyrrole-Based Porous Organic Polymers for Highly Efficient Iodine Capture

Xinru Wu,[1,#] *Zilong Wang,*[1,#] *Mengfan Wang,*[1,] *Xin Zheng,*[1,2] *Jiahong Pan,*[2] *Bing han,*[1,*] *Zhuoyu Ji,*[1,*]

[1] MOE Key Laboratory of Resources and Environmental Systems Optimization, College of Environmental Science and Engineering, North China Electric Power University, Beijing 102206, China

[2] State Key Laboratory of Featured Metal Materials and Life-Cycle Safety for Composite Structures, School of Resources, Environments and Materials, Guangxi University, Nanning 530004, China

[#] These authors contributed equally to this work.

* Corresponding authors.

E-mail: hanbing01@ncepu.edu.cn (Bing Han), jizhuoyu@ncepu.edu.cn (Zhuoyu Ji);

Table of Contents

1. **Materials and reagents** **3**

2. Synthesis process of C4P-POPs **5**

2.1 Synthesis of α,α,α,α-tetra(4-aminophenyl)calix[4]pyrrole (C4P) 5

2.2 Synthesis of C4P-Pl and C4P-Bto 5

2.3 Synthesis of C4P-Tab, C4P-Tp, C4P-Dp, C4P-Dha 6

3. Characterization **8**

4. Adsorption experiments **9**

4.1 Adsorption experiment of I_2 vapor and CH_3I 9

4.2 Adsorption experiment of iodine in liquid phase 9

4.3 Data fitting model 10

4.4 Stability experiments 11

4.5 The influence of ion competition 12

4.6 Recyclability experiments 12

5. Figure **14**

6. Table **28**

Reference **45**

1. Materials and reagents

Chemical Name	Purity	Manufacture
Pyrrole	99%	Aladdin Bio-Chem Technology Co., LTD
Methanesulfonic acid	99.5%	
4-Aminoacetophenone	99%	
Iodine	99.99%	
Potassium bromide	SP	
Sodium Chloride	99.99%	
Sodium nitrate	99%	
Ethanol	99.5%	
Acetic acid	99.8%	
Phloroglucinol (Pl)	99%	Adamas-beta Co., LTD
1,3,5-Benzenetricarbaldehyde (Tab)	99%	
2,5-Dihydroxyterephthalaldehyde (Dha)	98%	
Mesitylene	99%	
1,4-Dioxane	99%	
1,2,4,5-Benzenetetrol (Bto)	98%	Macklin Biochecal Co., Ltd.
2,4,6-trihydroxy-1,3,5-benzenetricarbaldehyde (Tp)	98%	
Sodium iodide	99.5%	
Sodium sulfate	99%	
Sodium carbonate	99.5%	
Sodium bicarbonate	99.5%	

Sodium acetate	99%	
Tetrahydrofuran	99.5%	
Triethylamine	99.5%	
cyclohexane	99.7%	
1,4-Phthalaldehyde (Dp)	99%	Meryer Chemical Technology Co., Ltd
Methyl iodide	98%	

All the chemicals purchased are analytical grade reagents and can be used without further purification.

2. Synthesis process of C4P-POPs

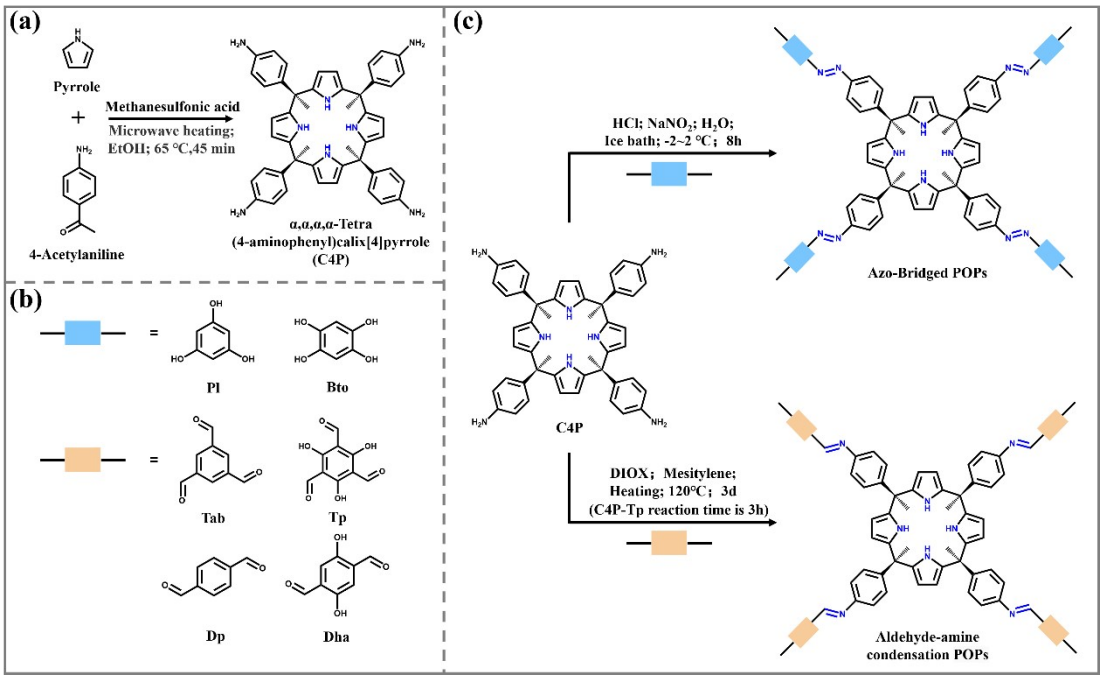

Scheme 1. Schematic diagram demonstrating the synthesis process of C4P–POPs. (a) Synthesis of α,α,α,α-tetra(4-aminophenyl)calix[4]pyrrole (C4P). (b) The specific co-monomers used to synthesize C4P-POPs. (c) The synthesis of C4P - POPs through azo-bridged and aldehyde-amine condensation reactions.

2.1 Synthesis of α,α,α,α-tetra(4-aminophenyl)calix[4]pyrrole (C4P)

4-Aminoacetophenone (1.5 mmol, 202.7 mg) and pyrrole (1.5 mmol, 105 μL) were mixed in 5mL ethanol, and methanesulfonic acid (100 μL) was added as a catalyst. The reaction mixture was subjected to microwave heating at 65 °C for 45 minutes. Upon completion, 50mL deionized water was added to the mixture, and triethylamine was slowly dropped into the mixture to adjust the pH to between 5-6. A significant quantity of pink precipitate formed in the solution. Subsequently, the C4P was filtered under reduced pressure and dried under vacuum at 65 °C.

2.2 Synthesis of C4P-Pl and C4P-Bto

In a typical synthesis, azo-bridged reaction needs to be carried out by preparing three solutions, specifically an acidic solution containing amine monomers, a $NaNO_2$ solution for the diazotization reaction, and an alkaline solution containing phenolic

monomers.

1. Acid dissolution: A mixture of deionized water (5 mL) and hydrochloric acid solution (1 mol·L^{-1}, 1 mL) was prepared and C4P (0.25 mmol, 186.25 mg) was added. Subsequently, the mixture was sonicated until complete dissolution of C4P, forming an acidic solution.

2. $NaNO_2$ solution preparation: Sodium nitrite ($NaNO_2$ 1.25 mmol, 61.3 mg) was dissolved in deionized water (1 mL) to form the $NaNO_2$ solution.

3. Alkaline solution preparation: Phloroglucinol (0.33 mmol, 42.0 mg) and sodium hydroxide (NaOH, 1.25 mmol, 50.0 mg) were dissolved in deionized water (1 mL) to obtain an alkaline solution.

Then all three solutions were cooled in an ice-water bath maintained at -2 to 2 °C. The $NaNO_2$ solution was added dropwise to the acidic C4P solution at -2-2 °C. The mixture was stirred for half an hour to make sure the diazonium process was complete. The resulting mixture was neutralized with alkaline solution, and added to the solution of diazonium mixture slowly at -2-2 °C. The reaction mixture was stirred for 8 h resulting in formation of a black precipitate. The solids were collected by filtration and

washed with dilute HCl, water, and ethanol, finally drying in a vacuum drying oven at 75 °C.

The synthesis of C4P-Bto is basically the same as the above-mentioned process (except that the ratio of C4P:Bto is 1:2).

2.3 Synthesis of C4P-Tab, C4P-Tp, C4P-Dp, C4P-Dha

C4P (0.25 mmol, 184.6 mg) and 1,3,5-triformylbenzene (0.33 mmol, 54.0 mg) were dissolved in a mixed organic solvent (1,4-dioxane: mesitylene=3:1, 20 mL). The solution was sonicated and bubbled with N_2 for 10 minutes. The reaction mixture was then transferred to a pressure flask and heated at 120 °C for 72 hours. After cooling, the product was washed and filtered three times respectively with water, ethanol, and tetrahydrofuran, finally drying in a vacuum drying oven at 75 °C for 12 hours to obtain C4P-Tab.

The synthesis of C4P-Tp is basically the same as the above-mentioned process (except that the reaction time is 3 h).The synthesis of C4P-Dp and C4P-Dha are the same as C4P-Tab process (except that the ratio of C4P:Dp or Dha is 1:2).

3. Characterization

Fourier transform infrared spectra (FTIR) of adsorbents were characterized by SHI-MADZU-IRT racer-100 spectrometer to determine the functional groups and their variations. The crystal structures were measured in an X-ray diffractometer (Rigaku SmartLab SE) with Cu Kα radiation operated in the 2θ range from 5° to 40°. The surface morphologies of the materials were observed with TESCAN MIRA LMS scanning electron microscope (SEM). The Brunauer-Emmett-Teller (BET) surface areas was characterized by the Micromeritics ASAP 2460 specific surface area and porosity analyzer to collect the N_2 adsorption/desorption isotherms collected at 77 K under a liquid nitrogen bath. Thermogravimetric analyses (TGA) were performed on NETZSCH STA 2500 at the temperature range of 25 to 800 ℃ under nitrogen atmosphere, the heating rate was 10 ℃·min^{-1}. The elemental analyses were conducted using Elementar (Germany), model UNICUBE CHNS/O analyser as per standards ASTM D 5291 and ASTM D1552. X-ray photoelectron spectroscopy (XPS) was carried out on Thermo Scientific ESCALAB 250Xi with an Al-alpha excitation source. The zeta potentials of the materials were tested through Malvern Panalytical ZEN 1002. The absorption spectra were recorded by Shimadzu, UV-2007 UV-vis absorption spectrometer.

4. Adsorption experiments

4.1 Adsorption experiment of I_2 vapor and CH_3I

The vapor phase iodine adsorption experiment was carried out in a closed environment (75 ℃, atmospheric pressure). By weighing method, the sealed container was removed at different time periods, and the adsorption performance of the adsorbent to gaseous phase iodine was determined by mass change. The specific steps are as follows: Prepare two 5 mL glass bottles, fill one empty bottle with a certain amount of adsorbent, and the other glass bottle as a blank control. After weighing the two glass bottles again, put them into a large airtight glass bottle containing iodine or iodomethane, and then place the large glass bottles in a constant temperature oven at 75 ℃. After a period of time, the glass bottles were removed from the oven and left to cool at room temperature. Two 5 mL glass bottles were taken out and weighed and recorded. The adsorption experiment was continued at 75 ℃ until the weight reached a stable value. Finally, the following formula was used to determine the adsorption amount of the adsorbent at a certain time.

$$q_t = \frac{(m_t - m_1) - (M_t - M_0)}{(m_1 - m_0)} \quad (1)$$

Where q_t ($g \cdot g^{-1}$) is static vapor capture at time t; m_t (g) is the weight of vial containing adsorbent at time t; m_1 (g) is the weight of vial containing adsorbent before adsorption; m_0 (g) is the weight of empty vial containing adsorbent; M_t (g) is the weight of control vial at time t; M_0 (g) is the weight of control vial.

4.2 Adsorption experiment of iodine in liquid phase

The solutions used in the liquid phase iodine adsorption experiment were all concentrated standard iodine solutions with deionized water or high purity solvent, and different concentrations of liquid iodine solutions were obtained by diluting the solvent. All the liquid phase iodine adsorption experiments were carried out at normal temperature and pressure.

The adsorption isotherm experiment is to dilute the mother liquor to a series of concentration gradients according to the experimental protocol. Then the adsorbent is dispersed in iodine aqueous solution with different initial concentration according to the set solid-liquid ratio, and then the glass bottle containing the mixture is placed in the shaking table. After 72 h of shock at room temperature, the materials can fully absorb the iodine in the solution and reach the adsorption equilibrium. After that, the materials and the solution were separated, and the absorbance of the solution is tested by ultraviolet spectrophotometer at 200-800 nm wavelength, and the iodine concentration before and after adsorption is determined according to the standard curve. Finally, the equilibrium amount of liquid phase iodine adsorbed by the materials was calculated using the following formula.

$$q_e = \frac{(C_0 - C_e) \times V}{m} \tag{2}$$

Where q_e ($mg \cdot g^{-1}$) is the equilibrium adsorption of iodine by the material; C_0 ($mg \cdot L^{-1}$) is the initial concentration of iodine in the solution; C_e ($mg \cdot L^{-1}$) is the equilibrium concentration of iodine in solution; V (L) is the volume of solution; m (g) is the weight of material.

The adsorption kinetics experiment is to disperse the material in liquid iodine solution according to a certain ratio of solid to liquid and stir it at room temperature. A bisection sample of the dispersion is collected at a specified time point and the material is separated from the solution. Then the absorbance of the solution is measured by ultraviolet-visible spectrophotometer at 200-800 nm wavelength, and the residual iodine concentration in the solution is obtained according to the standard curve. Finally, the liquid phase iodine's removal of material is calculated using the following formula.

$$\eta = \frac{(C_0 - C_t) \times 100\%}{C_0} \tag{3}$$

Where η (%) is the removal rate of iodine from the material in solution; C_0 ($mg \cdot L^{-1}$) is the initial concentration of iodine in the solution; C_t ($mg \cdot L^{-1}$) is the residual concentration of iodine in solution at time t.

4.3 Data fitting model

Langmuir and Freundlich isotherm fitting models are widely used in the simulation and analysis of isotherm adsorption data, through which adsorption types can be identified and adsorption properties of materials can be evaluated.

Langmuir isotherm:

$$\frac{C_e}{q_e} = \frac{1}{K_L q_m} + \frac{C_e}{q_m} \quad (4)$$

Freundlich isotherm:

$$\lg q_e = \lg K_F + \frac{1}{n}\lg C_e \quad (5)$$

Where q_m ($mg \cdot g^{-1}$) is the maximum adsorption capacity; K_L ($L \cdot mg^{-1}$) is the Langmuir model constant; n is the Freundlich constant; K_F ($L^{1/n} \cdot mg^{1-1/n} \cdot g^{-1}$) is the Freundlich constant; R^2 is the fitting coefficient.

Pseudo-first-order and pseudo-second-order kinetic models are widely used to simulate and analyze kinetic adsorption data.

Pseudo-first-order dynamics model:

$$ln(q_e - q_t) = lnq_e - k_1 t \quad (6)$$

Pseudo-second-order dynamics model：

$$\frac{t}{q_t} = \frac{1}{k_2 q_e^2} + \frac{t}{q_e} \quad (7)$$

Where k_1 is the rate constant of a pseudo-first-order kinetic model; k_2 is the rate constant of a pseudo-second-order kinetic model; q_t ($mg \cdot g^{-1}$) is the adsorption capacity at time t.

4.4 Stability experiments

In order to test the stability of the material, the materials were dispersed in strong acid solution (1 M and 3 M) HCl and HNO_3 aqueous solution, and strong alkali solution (1 M and 3 M) NaOH aqueous solution, respectively, and shaken in a shaker for 24h. The mixture was then filtered and thoroughly cleaned with deionized water. The

materials were then dried under vacuum at 75 ℃. Finally, the adsorption properties of the materials were characterized by ultraviolet and visible spectrophotometry (UV-Vis).

4.5 The influence of ion competition

In natural water and sewage, anions such as NO_3^-, Cl^-, SO_4^{2-}, HCO_3^-, AC^- may affected the I_3^- removal efficiency of the materials. Therefore, in order to simulate the coexistence of anions in water, NO_3^-, Cl^-, SO_4^{2-}, HCO_3^-, AC^- were added to I_3^- solution alone or mixed. The concentration of competitive anions in I_3^- in aqueous solution was 1 mol·L^{-1} and 50 mg·L^{-1} respectively (the competitive ion in the solution mixed with competitive ions was 5 mol L^{-1}), and the concentration of competitive anions was much higher than that of I_3^-. After the experimental solutions are treated, the materials are added to these solutions according to the solid-liquid ratio of adsorption kinetics. After 72 h of shaking in the shaker at room temperature, the absorbance of the material was measured by UV-Vis. Finally, the removal rate of I_3^- was calculated by using standard curve and Eq. (3) under the coexistence of competing anions and I_3^-.

4.6 Recyclability experiments

In order to test the recyclability of the material, the cyclic properties of the material were tested in iodine aqueous solution and iodine cyclohexane solution as follows:

(1) Iodine vapor cycle adsorption experiment

10 mg of the material was weighed as the adsorbent, and the method in section 2.2 was adopted in the adsorption test. It was placed in saturated gaseous iodine at 75 ℃ for 72 h to achieve saturated adsorption. After 72 h, after cooling from the oven, the adsorbed material was soaked in glass bottles with anhydrous ethanol and placed in the oven at 75 ℃. The solvent was exchanged several times within 24 h until the supernatant was clarified. The ethanol was filtered and washed and dried in a vacuum drying oven at 60 ℃ for 12 h, and then the next iodine vapor adsorption cycle was carried out.

(2) Cyclic adsorption experiment of iodine aqueous solution

The material was dispersed in 100 mL of 100 $mg \cdot L^{-1}$ iodine aqueous solution at a solid-liquid ratio of 0.08 $mg \cdot L^{-1}$ and placed in a shaker for 48 h. After filtration, the adsorbed material is obtained, and the absorbance of the filtrate is determined by the same method as above to obtain the adsorption efficiency of the material for iodine. The adsorbed material was soaked in a glass bottle with anhydrous ethanol and placed in an oven at 75 ℃. The solvent was exchanged several times within 24 h until the supernatant was clarified. The ethanol was filtered and washed and then dried in a vacuum drying oven at 60 ℃ for 12h, and then continued to the next iodine solution adsorption cycle.

(3) Cyclic adsorption experiment of iodine in cyclohexane solution

The material was dispersed in 100 ml of 250 $mg \cdot L^{-1}$ iodine aqueous solution at a solid-liquid ratio of 1.0 $g \cdot L^{-1}$ and placed in a shaker for 48h. After filtration, the adsorbed material is obtained, and the absorbance of the filtrate is determined by the same method as above to obtain the adsorption efficiency of the material for iodine. The adsorbed material was soaked in a glass bottle with anhydrous ethanol and placed in an oven at 75 ℃. The solvent was exchanged several times within 24 h until the supernatant was clarified. The ethanol was filtered and washed and then dried in a vacuum drying oven at 60 ℃ for 12 h, and then continued to the next cyclohexane solution adsorption cycle of iodine.

5. Figure

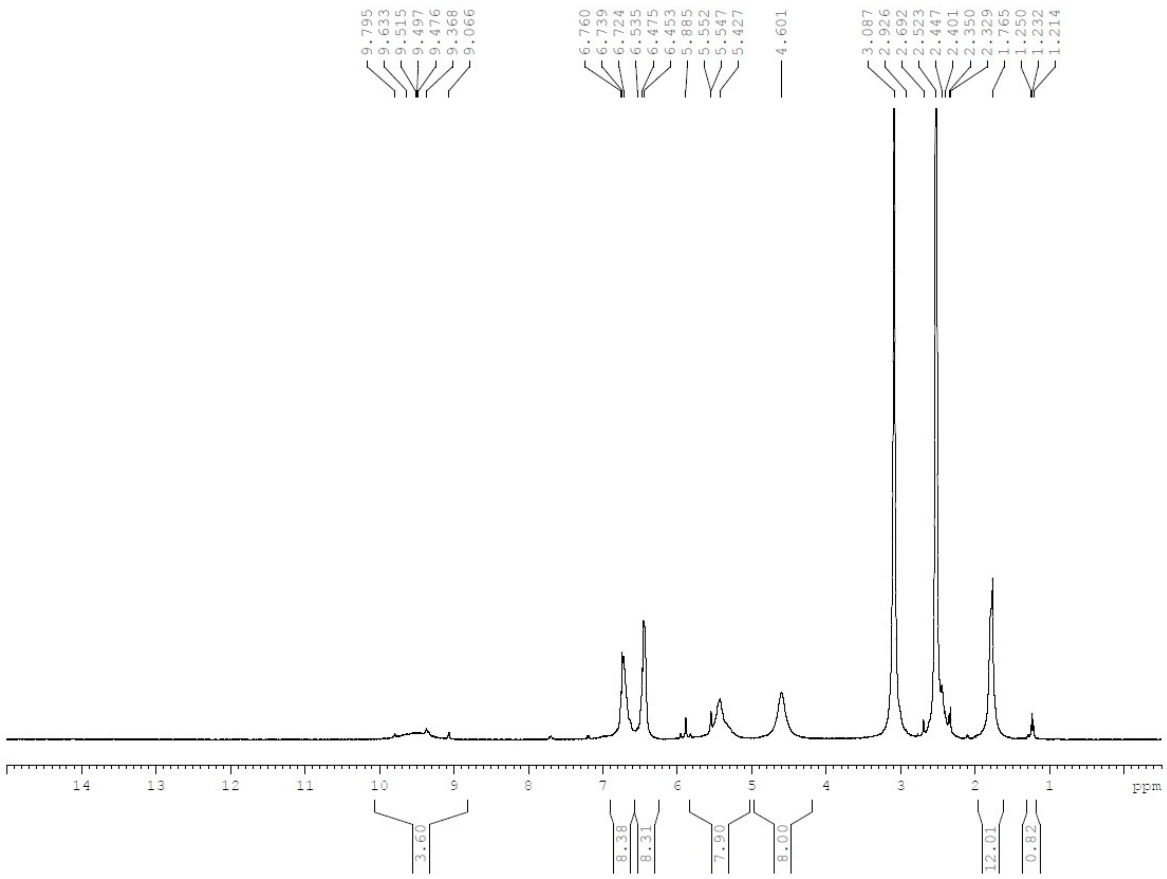

Figure S1 ^{1}H NMR spectra of C4P (400 MHz, DMSO-d6)

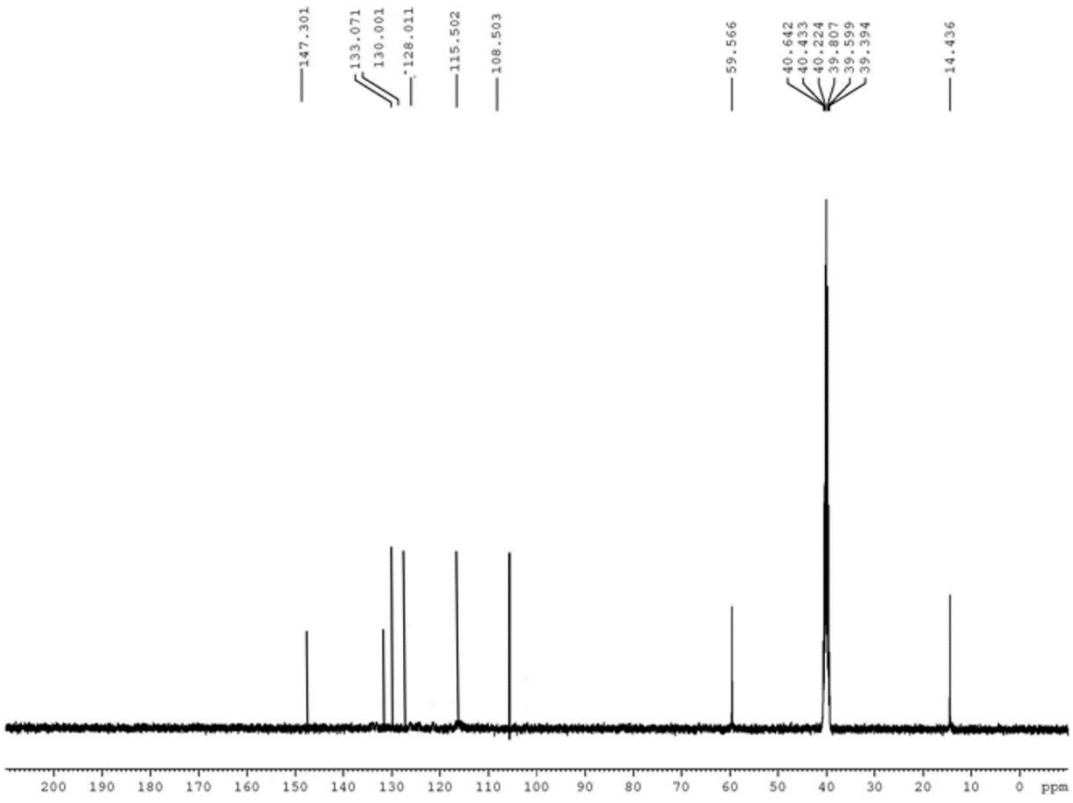

Figure S2 ^{13}C NMR spectra of C4P (400 MHz, DMSO-d6)

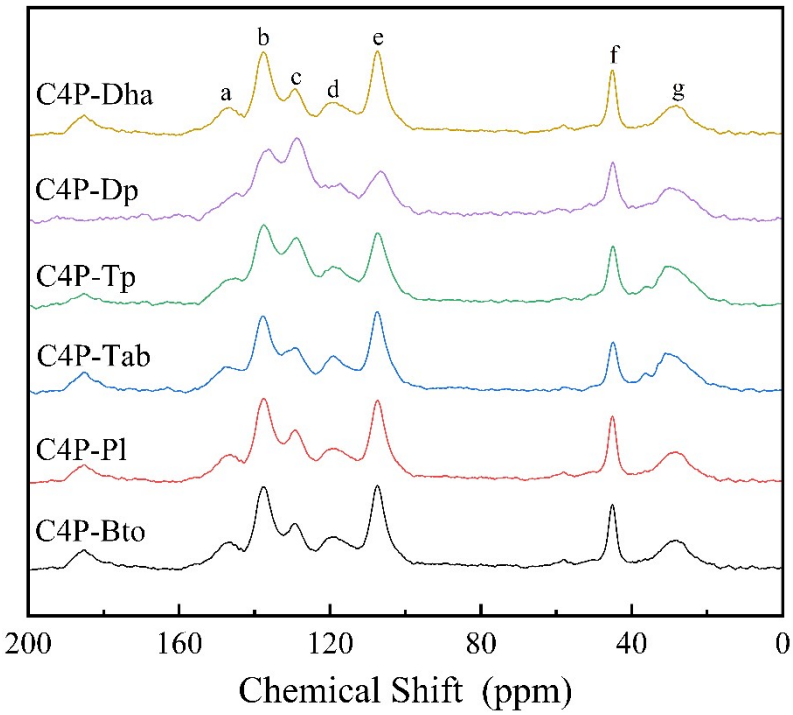

Figure S3 Solid-state ^{13}C NMR spectra of C4P-POPs

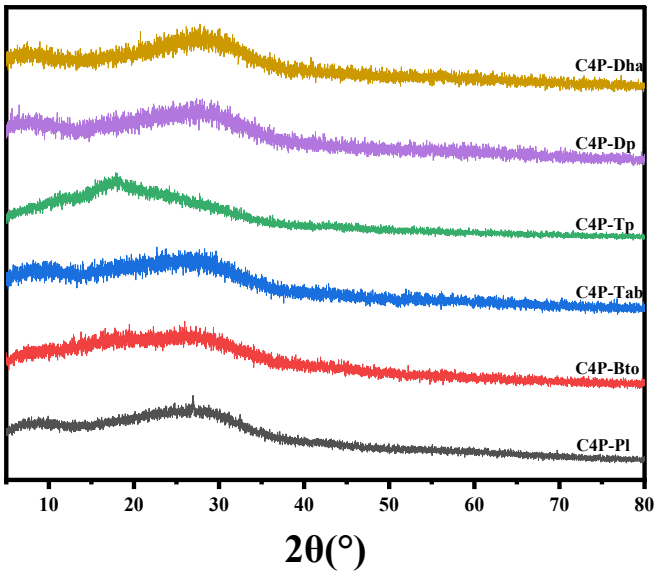

Figure S4. PXRD spectra of C4P-POPs.

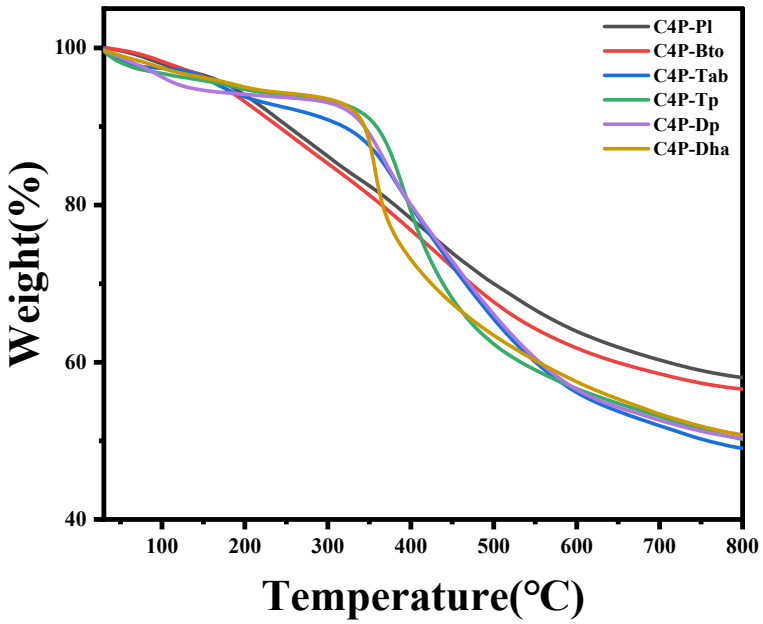

Figure S5. TGA curves for the different C4P-POPs. Samples were heated at 10 °C/min under a N_2 flow.

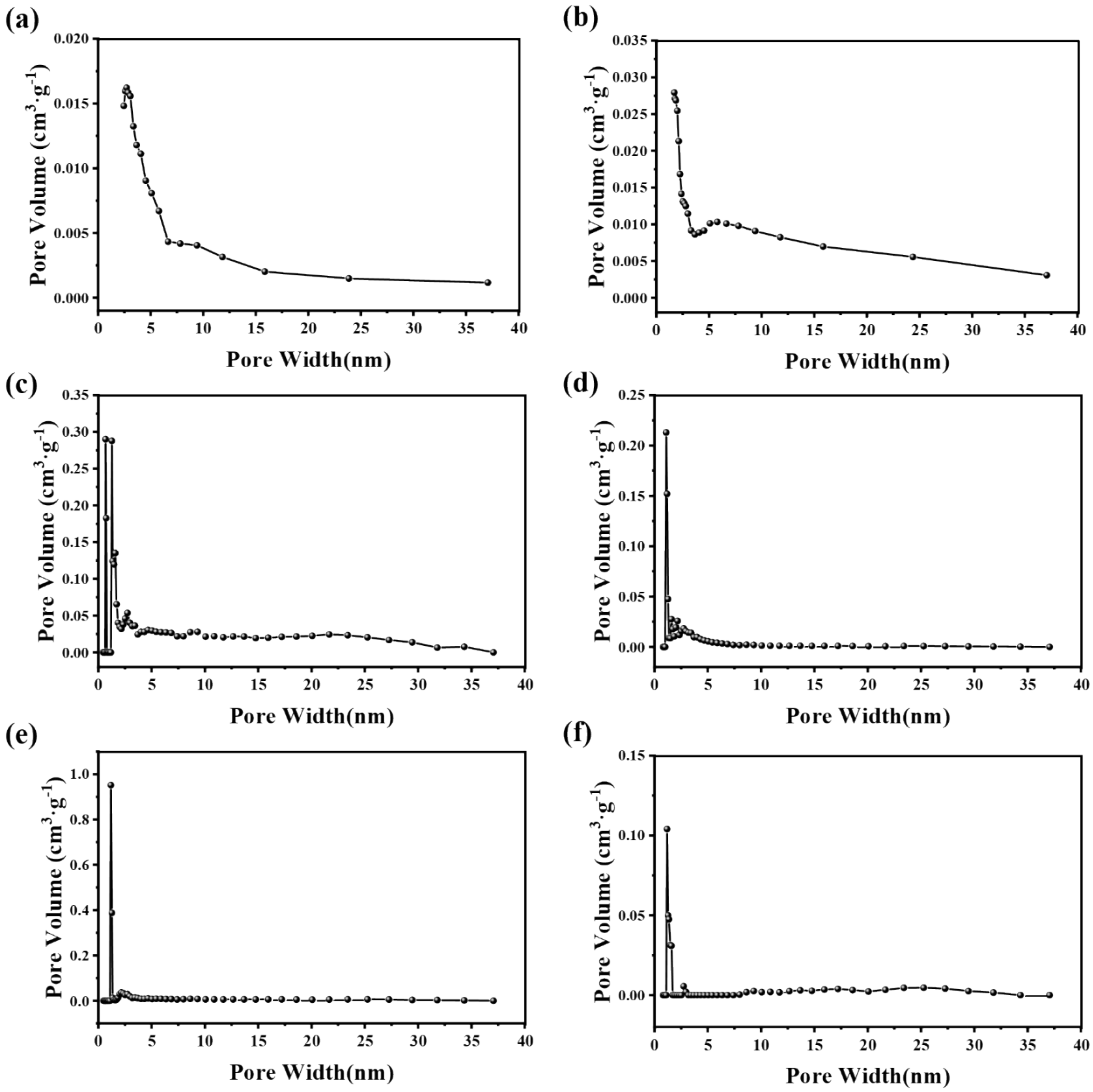

Figure S6. Pore size distributions measured at 77 K for (a) C4P-Pl, (b) C4P-Bto, (c) C4P-Tab, (d) C4P-Tp, (e) C4P-Dp, (f) C4P-Dha.

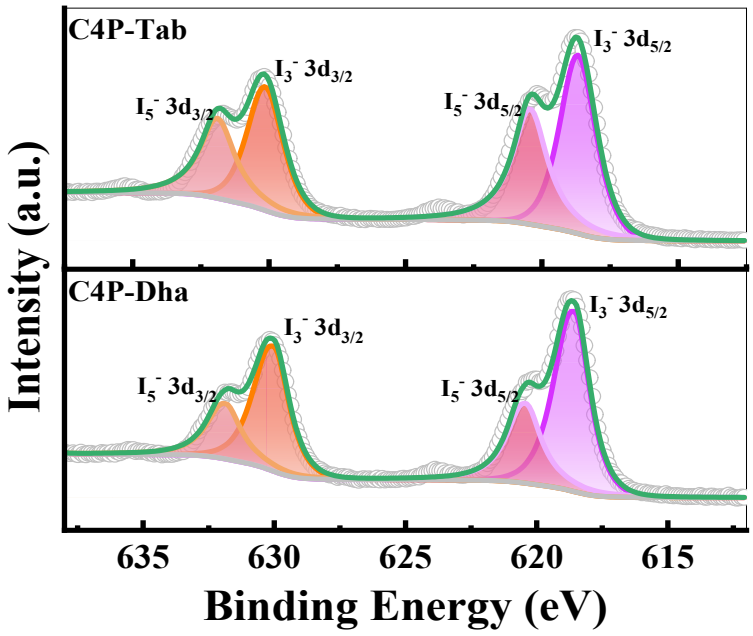

Figure S7. XPS after adsorption of I_2 vapor by C4P-Tab and C4P-Dha.

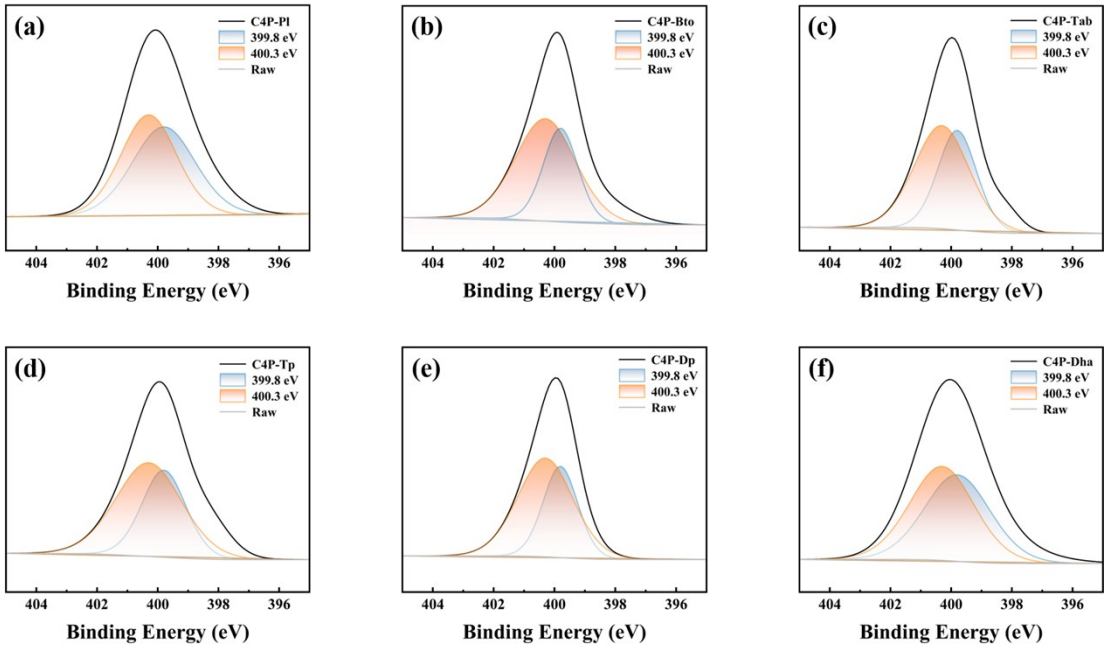

Figure S8 XPS spectra of N 1s of pristine C4P-POPs.

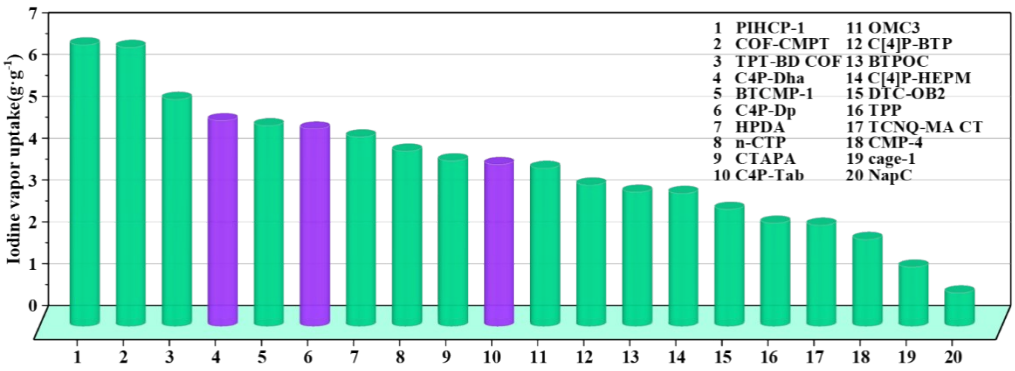

Figure S9. Comparison of the performance of different materials for I_2 vapor capture.

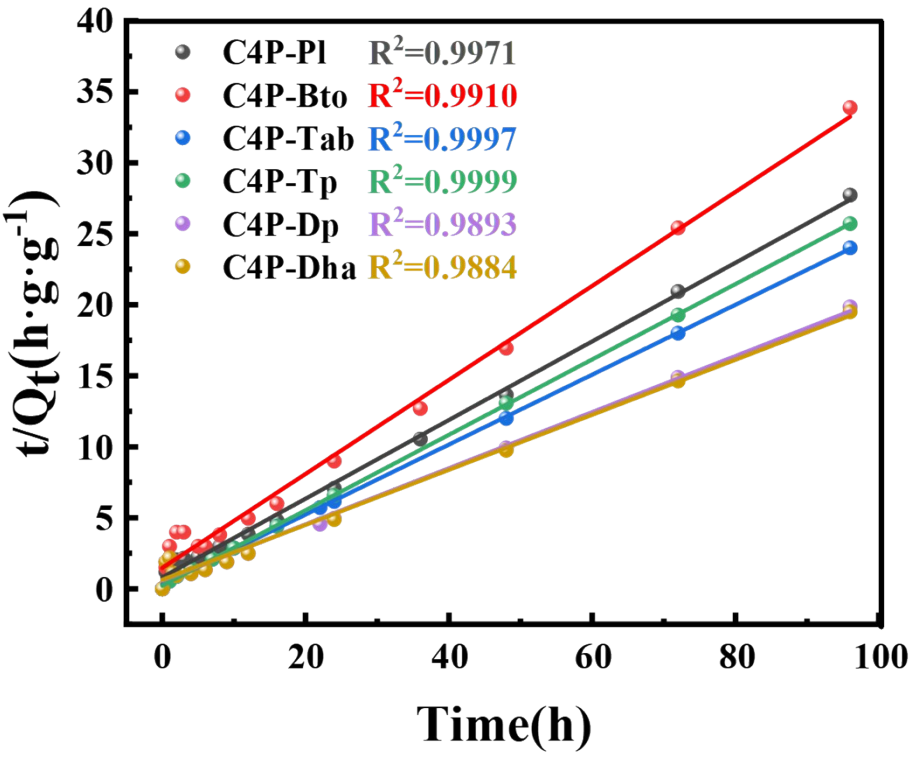

Figure S10. Pseudo-second-order adsorption kinetic plots of I_2 uptake by POPs.

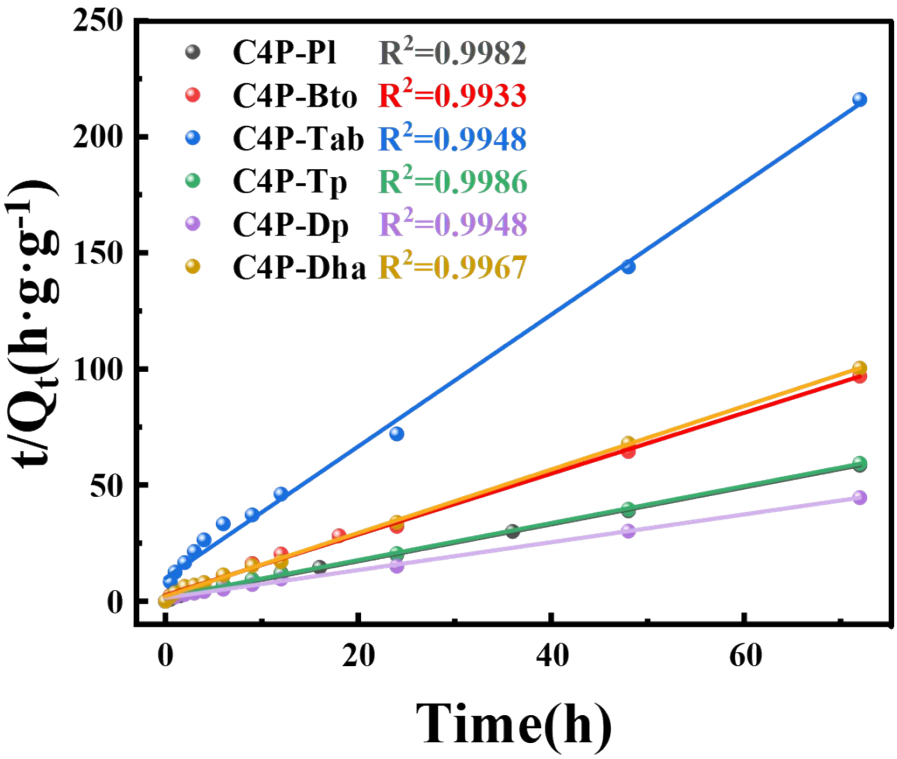

Figure S11. Pseudo-second-order adsorption kinetic plots of CH_3I uptake by POPs.

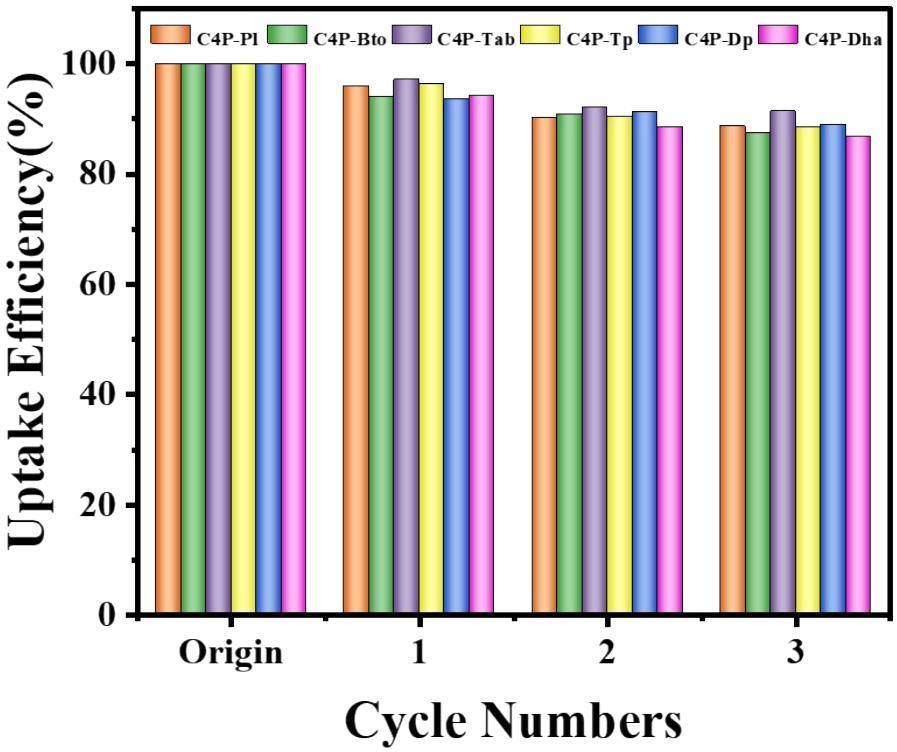

Figure S12. Recycle test data of C4P-POPs for static I_2 adsorption.

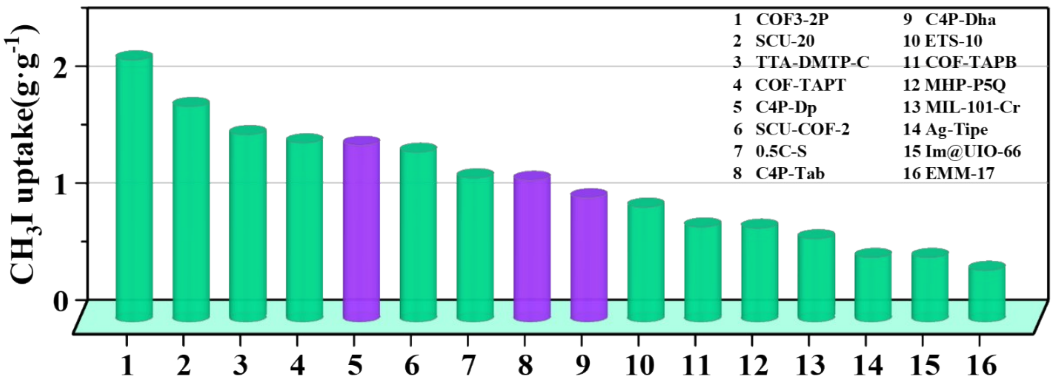

Figure S13. Comparison of the performance of different materials for CH_3I vapor capture.

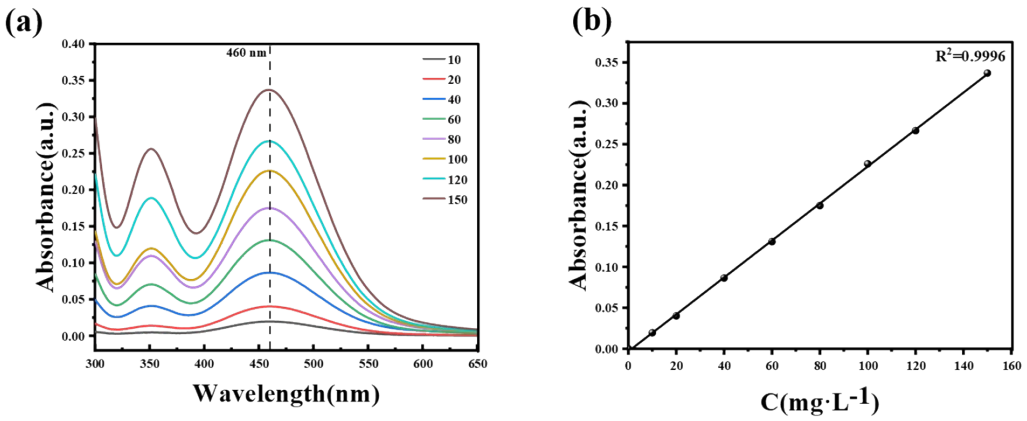

Figure S14. (a) UV-Vis spectra of iodine aqueous solution at different concentrations.

(b) Standard curve plotted based on the absorbance at 460 nm.

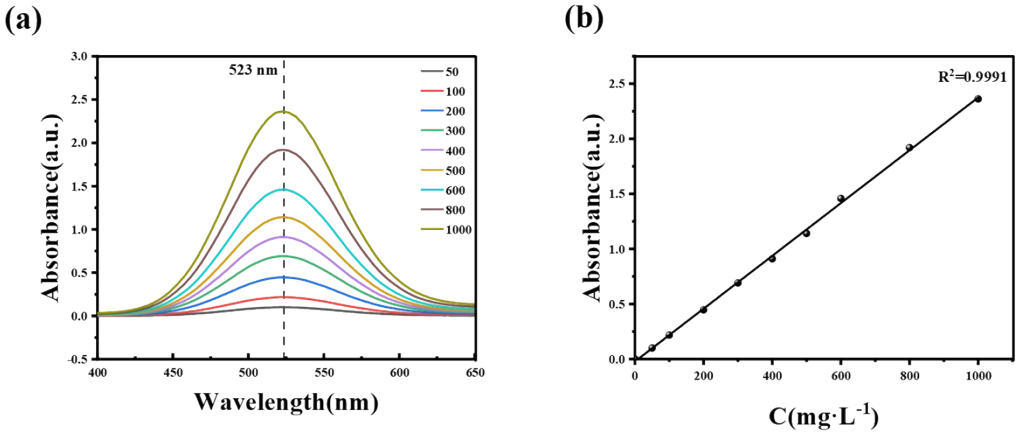

Figure S15. (a) UV-Vis spectra iodine cyclohexane solution at different concentrations.

(b) Standard curve plotted based on the absorbance at 523 nm.

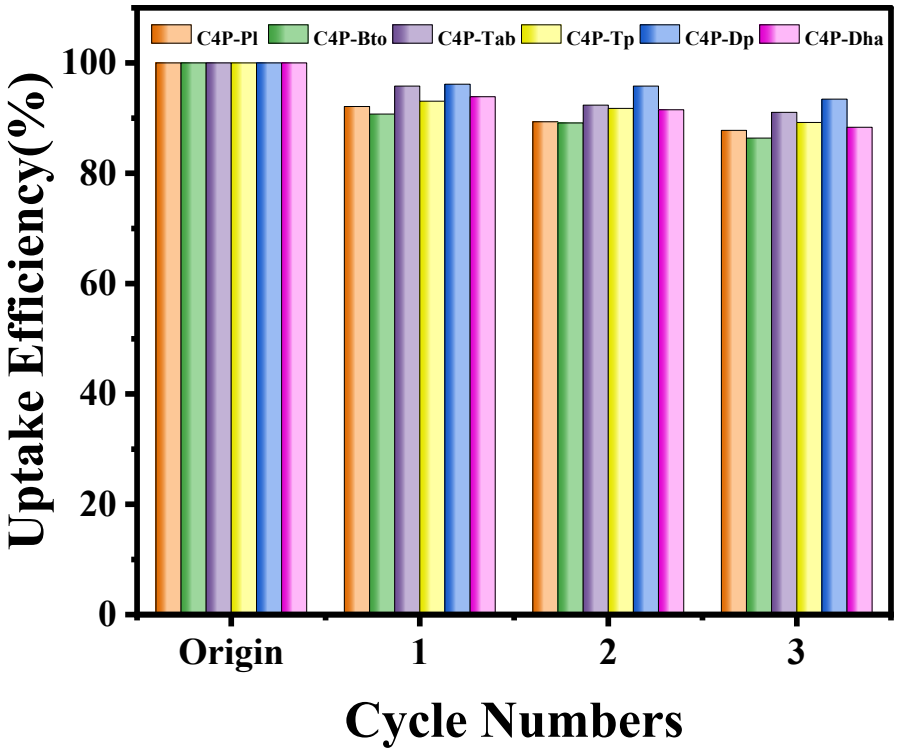

Figure S16. Recycle test data of C4P-POPs for iodine cyclohexane solution adsorption.

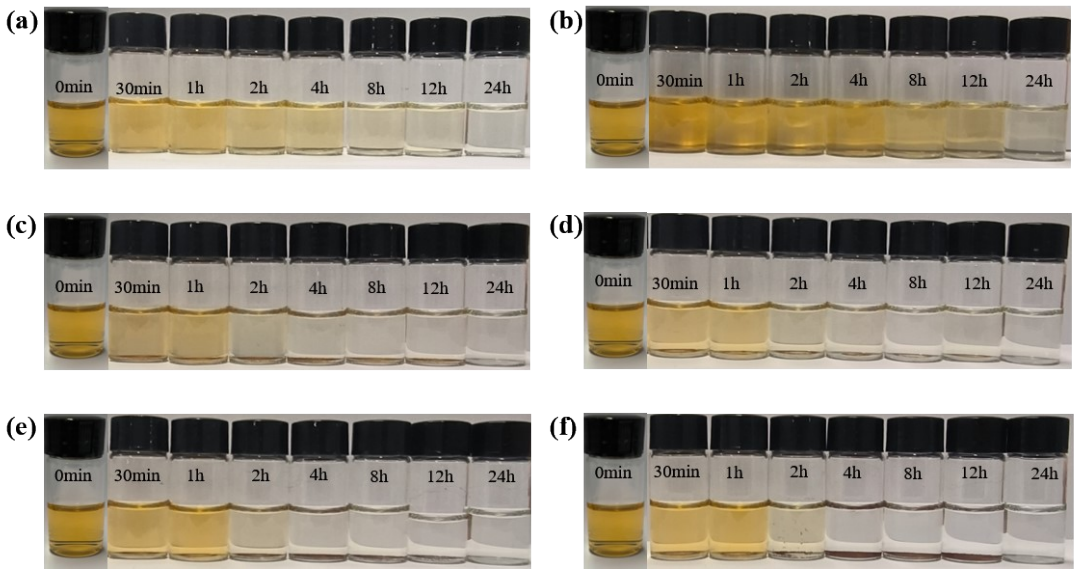

Figure S17. The color change of the iodine aqueous solution during the adsorption kinetic process. (a) C4P-Pl, (b) C4P-Bto, (c) C4P-Tab, (d) C4P-Tp, (e) C4P-Dp, (f) C4P-Dha.

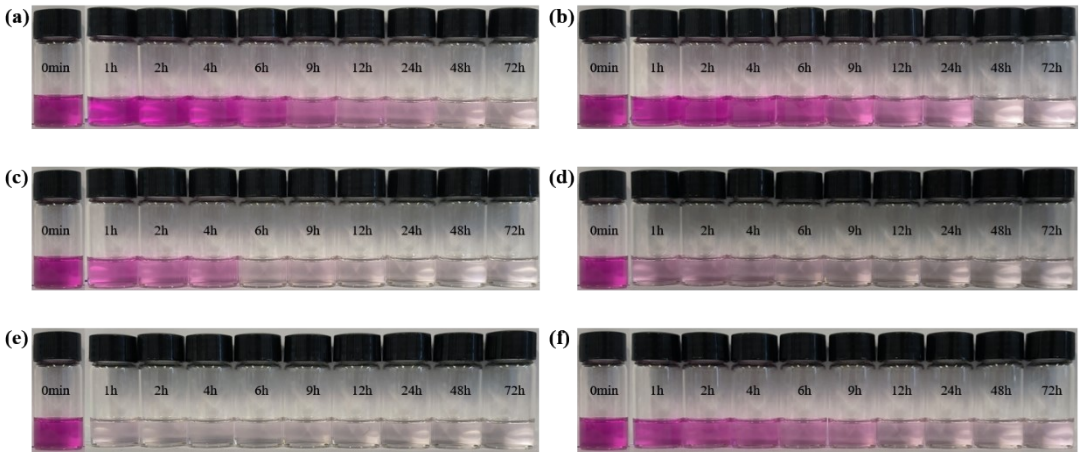

Figure S18. The color change of the iodine cyclohexane solution during the adsorption kinetic process. (a) C4P-Pl, (b) C4P-Bto, (c) C4P-Tab, (d) C4P-Tp, (e) C4P-Dp, (f) C4P-Dha.

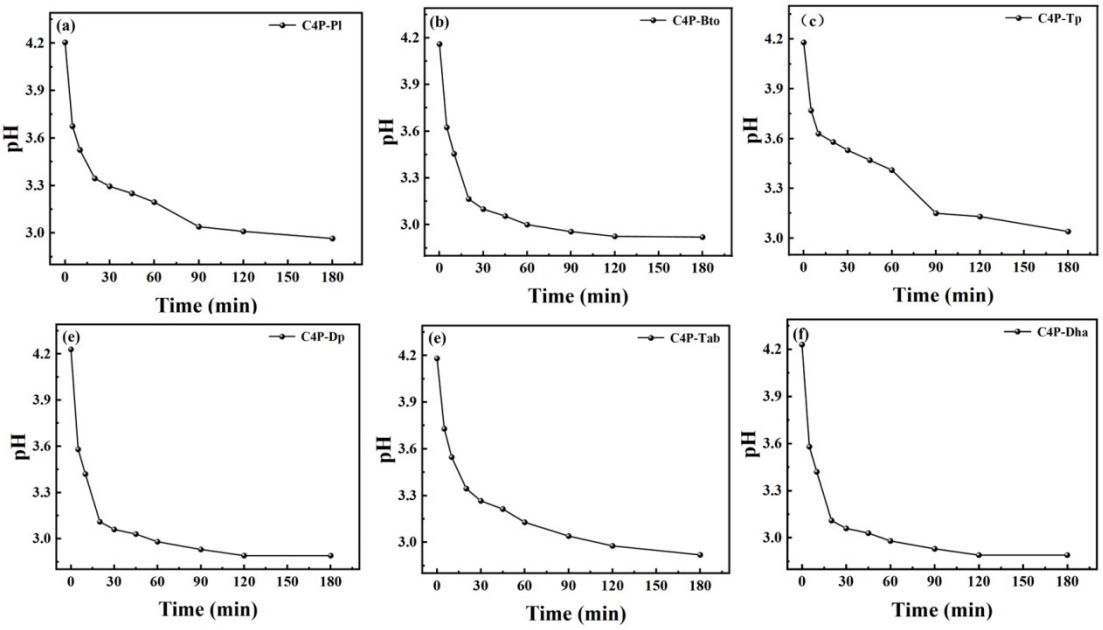

Figure S19. The pH evolution of iodine solution（100 ppm） during the adsorption process.

6. Table

Table S1. Elemental Analysis of C4P-POPs

C4P-POPs	C (%)	H (%)	N (%)
C4P-Pl	73.13	5.69	14.20
C4P-Bto	69.08	5.21	13.46
C4P-Tab	81.75	5.49	12.72
C4P-Tp	80.33	5.39	12.48
C4P-Dp	79.3	5.83	11.56
C4P-Dha	79.64	5.43	11.61

Table S2. BET surface area and porosity parameters of the C4P-POPs considered in the present study.

Sample	BET surface area ($m^2 \cdot g^{-1}$)[a]	Pore volume ($cm^3 \cdot g^{-1}$)[b]	Pore Width (nm)
C4P-Pl	179.5	0.561	2.72
C4P-Bto	148.2	0.241	1.86
C4P-Tab	629.9	1.12	1.27
C4P-Tp	210.2	0.155	1.58
C4P-Dp	442.6	0.534	1.18
C4P-Dha	195.7	0.431	1.18

[a] BET surface areas determined by N_2 adsorption at 77 K.

[b] total pore volumes determined by N_2 adsorption at 77 K.

Table S3. Iodine vapor adsorption equilibrium time and uptake volume of C4P-POPs.

Sample	Equilibrium Time(h)	Iodine Uptake($g \cdot g^{-1}$)
C4P-Pl	72	3.45
C4P-Bto	48	3.08
C4P-Tab	48	3.87
C4P-Tp	96	3.79
C4P-Dp	12	4.72
C4P-Dha	24	4.92

Table S4. Adsorption kinetics parameters for idoine vapor uptake by C4P-POPs.

Sample	Pseudo-first-order		Pseudo-second-order	
C4P-Pl	q_e ($g \cdot g^{-1}$)	3.46	q_e ($g \cdot g^{-1}$)	3.61
	K_1 (h^{-1})	0.175	K_2 ($g \cdot g^{-1} \cdot h^{-1}$)	0.0938
	R^2	0.990	R^2	0.997
C4P-Bto	q_e ($g \cdot g^{-1}$)	3.09	q_e ($g \cdot g^{-1}$)	3.02
	K_1 (h^{-1})	0.163	K_2 ($g \cdot g^{-1} \cdot h^{-1}$)	0.0739
	R^2	0.990	R^2	0.991
C4P-Tab	q_e ($g \cdot g^{-1}$)	3.71	q_e ($g \cdot g^{-1}$)	4.06
	K_1 (h^{-1})	0.463	K_2 ($g \cdot g^{-1} \cdot h^{-1}$)	0.192
	R^2	0.973	R^2	0.997
C4P-Tp	q_e ($g \cdot g^{-1}$)	3.52	q_e ($g \cdot g^{-1}$)	3.77
	K_1 (h^{-1})	0.508	K_2 ($g \cdot g^{-1} \cdot h^{-1}$)	0.302
	R^2	0.986	R^2	0.999
C4P-Dp	q_e ($g \cdot g^{-1}$)	4.78	q_e ($g \cdot g^{-1}$)	5.06
	K_1 (h^{-1})	0.304	K_2 ($g \cdot g^{-1} \cdot h^{-1}$)	0.0655
	R^2	0.981	R^2	0.9893
C4P-Dha	q_e ($g \cdot g^{-1}$)	4.99	q_e ($g \cdot g^{-1}$)	5.16
	K_1 (h^{-1})	0.278	K_2 ($g \cdot g^{-1} \cdot h^{-1}$)	0.590
	R^2	0.978	R^2	0.9884

Table S5. Comparison of the iodine vapor adsorption capacity between C4P-POPs and reported adsorbents.

Sample	Equilibrium Time(h)	Iodine Uptake($g \cdot g^{-1}$)	Ref.
PIHCP-1	24	6.73	1
COF-TMPT	24	6.67	2
TPT-BD COF	48	5.43	3
C4P-Dha	24	4.92	This work
BTCMP-1	12	4.8	4
C4P-Dp	12	4.72	This work
HPDA	60	4.53	5
n-CTP	21	4.19	6
CTAPA	72	3.96	7
C4P-Tab	48	3.87	This work
OMC3	12	3.78	8
C[4]P-BTP	4	3.38	9
BTPOC	15	3.21	10
C[4]P-HEPM	5	3.18	11
DTC-OB2	3	2.8	12
TPP	1.5	2.47	13
TCNQ-MA CTC	32	2.42	14
CMP-4	20	2.08	15
cage-1	36	1.42	16
NapC	6	0.8	17

Table S6. CH_3I vapor adsorption equilibrium time and uptake volume of C4P-POPs.

Sample	**Equilibrium Time(h)**	**CH_3I Uptake($g \cdot g^{-1}$)**
C4P-Pl	96	0.97
C4P-Bto	96	0.79
C4P-Tab	72	1.21
C4P-Tp	72	0.52
C4P-Dp	72	1.51
C4P-Dha	72	1.06

Table S7. Adsorption kinetics parameters for CH_3I uptake by C4P-POPs.

Sample	Pseudo-first-order		Pseudo-second-order	
C4P-Pl	q_e ($g \cdot g^{-1}$)	0.87	q_e ($g \cdot g^{-1}$)	1.26
	K_1 (h^{-1})	0.179	K_2 ($g \cdot g^{-1} \cdot h^{-1}$)	0.474
	R^2	0.897	R^2	0.998
C4P-Bto	q_e ($g \cdot g^{-1}$)	0.68	q_e ($g \cdot g^{-1}$)	0.76
	K_1 (h^{-1})	0.307	K_2 ($g \cdot g^{-1} \cdot h^{-1}$)	0.670
	R^2	0.893	R^2	0.993
C4P-Tab	q_e ($g \cdot g^{-1}$)	1.13	q_e ($g \cdot g^{-1}$)	0.35
	K_1 (h^{-1})	0.227	K_2 ($g \cdot g^{-1} \cdot h^{-1}$)	0.810
	R^2	0.960	R^2	0.995
C4P-Tp	q_e ($g \cdot g^{-1}$)	0.49	q_e ($g \cdot g^{-1}$)	1.25
	K_1 (h^{-1})	0.070	K_2 ($g \cdot g^{-1} \cdot h^{-1}$)	0.361
	R^2	0.867	R^2	0.999
C4P-Dp	q_e ($g \cdot g^{-1}$)	1.39	q_e ($g \cdot g^{-1}$)	1.67
	K_1 (h^{-1})	0.283	K_2 ($g \cdot g^{-1} \cdot h^{-1}$)	0.252
	R^2	0.941	R^2	0.995
C4P-Dha	q_e ($g \cdot g^{-1}$)	0.974	q_e ($g \cdot g^{-1}$)	0.73
	K_1 (h^{-1})	0.129	K_2 ($g \cdot g^{-1} \cdot h^{-1}$)	0.880
	R^2	0.914	R^2	0.997

Table S8. Comparison of the CH_3I adsorption capacity between C4P-POPs and reported adsorbents.

Sample	Iodine Uptake($g \cdot g^{-1}$)	Ref.
COF3-2P	2.24	18
SCU-20	1.84	19
TTA-DMTP-COF	1.6	20
COF-TAPT	1.53	21
C4P-Dp	1.51	This work
SCU-COF-2	1.45	22
0.5C-S	1.23	23
C4P-Tab	1.21	This work
C4P-Dha	1.06	This work
ETS-10	0.98	24
COF-TAPB	0.81	21
MHP-P5Q	0.8	25
MIL-101-Cr-TED	0.71	26
Ag-Tipe	0.55	27
Im@UiO-66	0.55	28
EMM-17	0.44	29

Table S9. Iodine aqueous solution adsorption equilibrium time and capture volume of C4P-POPs.

Sample	**Equilibrium Time(h)**	**q_{max}($g \cdot g^{-1}$)**
C4P-Pl	27	2.77
C4P-Bto	27	3.01
C4P-Tab	24	3.96
C4P-Tp	24	2.63
C4P-Dp	24	2.93
C4P-Dha	12	3.70

Table S10. Adsorption kinetics parameters for iodine aqueous solution capture by C4P-POPs.

Sample	Langmuir model[a]		Freundlich model[b]	
C4P-Pl	q_e ($g \cdot g^{-1}$)	2.77	K_F	364.79
	K_L	0.0380	1/n	0.396
	R^2	0.970	R^2	0.975
C4P-Bto	q_e ($g \cdot g^{-1}$)	3.01	K_F	379.86
	K_L	0.0443	1/n	0.419
	R^2	0.893	R^2	0.920
C4P-Tab	q_e ($g \cdot g^{-1}$)	3.96	K_F	936.32
	K_L	0.128	1/n	0.369
	R^2	0.950	R^2	0.995
C4P-Tp	q_e ($g \cdot g^{-1}$)	2.63	K_F	776.61
	K_L	0.190	1/n	0.285
	R^2	0.967	R^2	0.930
C4P-Dp	q_e ($g \cdot g^{-1}$)	2.93	K_F	920.91
	K_L	0.197	1/n	0.273
	R^2	0.957	R^2	0.903
C4P-Dha	q_e ($g \cdot g^{-1}$)	3.70	K_F	919.21
	K_L	0.0930	1/n	0.301
	R^2	0.882	R^2	0.779

[a]K_L ($L \cdot mg^{-1}$) is the Langmuir model constant.

[b]K_F ($L^{1/n} \cdot mg^{1-1/n} \cdot g^{-1}$) is the Freundlich constant; 1/n is the inverse of Freundlich constant.

Table S11 Adsorption isotherm fitting parameters of C4P-POPs for iodine aqueous solution.

Sample	Pseudo-first-order		Pseudo-second-order	
C4P-Pl	q_e ($g \cdot g^{-1}$)	0.824	q_e ($g \cdot g^{-1}$)	1.000
	K_1 (h^{-1})	0.247	K_2 ($g \cdot g^{-1} \cdot min^{-1}$)	0.00418
	R^2	0.773	R^2	0.9993
C4P-Bto	q_e ($g \cdot g^{-1}$)	0.858	q_e ($g \cdot g^{-1}$)	1.003
	K_1 (h^{-1})	0.108	K_2 ($g \cdot g^{-1} \cdot min^{-1}$)	0.00376
	R^2	0.820	R^2	0.9995
C4P-Tab	q_e ($g \cdot g^{-1}$)	0.899	q_e ($g \cdot g^{-1}$)	0.975
	K_1 (h^{-1})	0.0174	K_2 ($g \cdot g^{-1} \cdot min^{-1}$)	0.00249
	R^2	0.970	R^2	0.9996
C4P-Tp	q_e ($g \cdot g^{-1}$)	0.860	q_e ($g \cdot g^{-1}$)	0.963
	K_1 (h^{-1})	0.0160	K_2 ($g \cdot g^{-1} \cdot min^{-1}$)	0.00203
	R^2	0.961	R^2	0.9990
C4P-Dp	q_e ($g \cdot g^{-1}$)	0.912	q_e ($g \cdot g^{-1}$)	0.970
	K_1 (h^{-1})	0.0202	K_2 ($g \cdot g^{-1} \cdot min^{-1}$)	0.00276
	R^2	0.970	R^2	0.9995
C4P-Dha	q_e ($g \cdot g^{-1}$)	0.946	q_e ($g \cdot g^{-1}$)	0.986
	K_1 (h^{-1})	0.0242	K_2 ($g \cdot g^{-1} \cdot min^{-1}$)	0.00215
	R^2	0.961	R^2	0.9933

Table S12 Comparison of the iodine aqueous solution adsorption capacity between C4P-POPs and reported adsorbents.

Sample	Iodine Uptake($g \cdot g^{-1}$)	Ref.
COFamide-1	4.6	30
C4P-Tab	3.96	This work
N-MOF-PAN	3.5	31
C4P-Dha	3.70	This work
C[4]P-BTP	3.03	9
C4P-Dp	2.93	This work
C[4]P-BP	2.31	9
Ag@MIL-101	2.14	32
NapC	1.97	17
PCN-223-HPP	1.68	33
Fe_3O_4@PPy	1.63	34
PCN-223	1.62	33
PTEP	1.45	35
DTC-OP3	1.25	12
DTC-OP2	1.11	12
BOF-1	0.93	36
MBM	0.88	37
ITN-POP	0.19	38
Ag-MSHC-6	0.077	39
PIHCP-1	0.033	1

Table S13. Iodine cyclohexane solution adsorption equilibrium time and capture volume of C4P-POPs.

Sample	**Equilibrium Time(h)**	**q_{max}($g \cdot g^{-1}$)**
C4P-Pl	48	0.66
C4P-Bto	48	0.20
C4P-Tab	24	2.24
C4P-Tp	24	1.55
C4P-Dp	1	1.40
C4P-Dha	24	1.23

Table S14. Adsorption kinetics parameters for Iodine cyclohexane solution capture by C4P-POPs.

Sample	Langmuir model[a]		Freundlich model[b]	
C4P-Pl	q_e ($g \cdot g^{-1}$)	0.66	K_F	20.38
	K_L	0.00430	1/n	0.498
	R^2	0.992	R^2	0.970
C4P-Bto	q_e ($g \cdot g^{-1}$)	0.20	K_F	4.35
	K_L	0.00313	1/n	0.532
	R^2	0.973	R^2	0.892
C4P-Tab	q_e ($g \cdot g^{-1}$)	2.24	K_F	82.72
	K_L	0.00609	1/n	0.499
	R^2	0.999	R^2	0.980
C4P-Tp	q_e ($g \cdot g^{-1}$)	1.55	K_F	76.15
	K_L	0.00658	1/n	0.450
	R^2	0.994	R^2	0.960
C4P-Dp	q_e ($g \cdot g^{-1}$)	1.42	K_F	112.56
	K_L	0.0125	1/n	0.399
	R^2	0.987	R^2	0.975
C4P-Dha	q_e ($g \cdot g^{-1}$)	1.23	K_F	96.92
	K_L	0.00947	1/n	0.379
	R^2	0.991	R^2	0.959

[a]K_L ($L \cdot mg^{-1}$) is the Langmuir model constant.

[b]K_F ($L^{1/n} \cdot mg^{1-1/n} \cdot g^{-1}$) is the Freundlich constant; 1/n is the inverse of Freundlich constant.

Table S15. Adsorption isotherm fitting parameters of C4P-POPs for iodine cyclohexane solution.

Sample	Pseudo-first-order		Pseudo-second-order	
C4P-Pl	q_e ($g \cdot g^{-1}$)	0.193	q_e ($g \cdot g^{-1}$)	0.193
	K_1 (min^{-1})	0.00193	K_2 ($g \cdot g^{-1} \cdot min^{-1}$)	0.000092
	R^2	0.989	R^2	0.999
C4P-Bto	q_e ($g \cdot g^{-1}$)	0.189	q_e ($g \cdot g^{-1}$)	0.195
	K_1 (min^{-1})	0.00198	K_2 ($g \cdot g^{-1} \cdot min^{-1}$)	0.000047
	R^2	0.995	R^2	0.98
C4P-Tab	q_e ($g \cdot g^{-1}$)	0.191	q_e ($g \cdot g^{-1}$)	0.197
	K_1 (min^{-1})	0.0256	K_2 ($g \cdot g^{-1} \cdot min^{-1}$)	0.000282
	R^2	0.977	R^2	0.996
C4P-Tp	q_e ($g \cdot g^{-1}$)	0.191	q_e ($g \cdot g^{-1}$)	0.196
	K_1 (min^{-1})	0.0689	K_2 ($g \cdot g^{-1} \cdot min^{-1}$)	0.000748
	R^2	0.993	R^2	0.999
C4P-Dp	q_e ($g \cdot g^{-1}$)	0.196	q_e ($g \cdot g^{-1}$)	0.196
	K_1 (min^{-1})	0.140	K_2 ($g \cdot g^{-1} \cdot min^{-1}$)	0.00957
	R^2	0.999	R^2	0.999
C4P-Dha	q_e ($g \cdot g^{-1}$)	0.177	q_e ($g \cdot g^{-1}$)	0.192
	K_1 (min^{-1})	0.0199	K_2 ($g \cdot g^{-1} \cdot min^{-1}$)	0.000149
	R^2	0.937	R^2	0.999

Table S16. Comparison of the iodine cyclohexane solution adsorption capacity between C4P-POPs and reported adsorbents.

Sample	Iodine Uptake($g \cdot g^{-1}$)	Ref.
C4P-Tab	2.24	This work
HCOF-1	2.10	40
C4P-Tp	1.55	This work
MFM-300(Sc)	1.54	41
HMTI-1	1.50	42
C4P-Dp	1.22	This work
TMU-15	1.30	43
UiO-66-PYDC	1.25	44
mICOP-1	1.15	45
Th-BDAT	1.05	46
MFM-300(Al)	0.94	41
COF-5d	0.91	47
$0.5Cu^0$-SBA-15	0.84	48
PA-PR	0.76	49
ICOP-1	0.70	45
TpBD-Me_2	0.68	50
SCNU-Z8(Ni)	0.64	51
ADLC	0.35	52
FMC3	0.17	53
PBC800	0.073	53

Table S17. Adsorption isotherm fitting parameters of C4P-POPs for I_3^-.

Sample	Pseudo-first-order		Pseudo-second-order	
C4P-Pl	q_e (mg·g^{-1})	44.15	q_e (mg·g^{-1})	45.83
	K_1 (min^{-1})	0.0248	K_2 (g·g^{-1}·min^{-1})	0.00111
	R^2	0.991	R^2	0.996
C4P-Bto	q_e (mg·g^{-1})	40.70	q_e (mg·g^{-1})	43.78
	K_1 (min^{-1})	0.0188	K_2 (g·g^{-1}·min^{-1})	0.00086
	R^2	0.980	R^2	0.994
C4P-Tab	q_e (mg·g^{-1})	42.34	q_e (mg·g^{-1})	43.82
	K_1 (min^{-1})	0.0889	K_2 (g·g^{-1}·min^{-1})	0.00519
	R^2	0.983	R^2	0.999
C4P-Tp	q_e (mg·g^{-1})	44.28	q_e (mg·g^{-1})	44.68
	K_1 (min^{-1})	0.0615	K_2 (g·g^{-1}·min^{-1})	0.00352
	R^2	0.955	R^2	0.998
C4P-Dp	q_e (mg·g^{-1})	44.29	q_e (mg·g^{-1})	44.35
	K_1 (min^{-1})	0.651	K_2 (g·g^{-1}·min^{-1})	0.243
	R^2	0.999	R^2	0.999
C4P-Dha	q_e (mg·g^{-1})	43.67	q_e (mg·g^{-1})	43.50
	K_1 (min^{-1})	0.121	K_2 (g·g^{-1}·min^{-1})	0.00315
	R^2	0.991	R^2	0.999

REFERENCES

1. J. Wang, T. Wu, X. Wang, J. Chen, M. Fan, Z. Shi, J. Liu, L. Xu and Y. Zang, *iScience*, 2024, **27**, 108993.
2. Y. Tang, Z. He, W. Xue, H. Huang and G. Zhang, *Chemical Engineering Journal*, 2023, **470**.
3. X. Guo, Y. Tian, M. Zhang, Y. Li, R. Wen, X. Li, X. Li, Y. Xue, L. Ma and C. Xia, *Chemistry of Materials*, 2018, **30**, 2299-2308.
4. L. Wang, W. Xie, G. Xu, S. Zhang, C. Yao and Y. Xu, *Polymers for Advanced Technologies*, 2021, **33**, 584-590.
5. F. Wang, T. Geng, X. Fang and H. Xu, *Journal of Applied Polymer Science*, 2022, **139**.
6. Y. Huang, W. Li, Y. Xu, M. Ding, J. Ding, Y. Zhang, Y. Wang, S. Chen, Y. Jin and C. Xia, *New Journal of Chemistry*, 2021, **45**, 5363-5370.
7. H. Zhu, Y. Qin, Y. Guo, Z. Shen, M. Imran, M. Asim Mushtaq, Z. Zhang, C. Ni, Y. Chen, Y. Ding, H. Gul, J. Zou, P. Tsiakaras, H.-Y. Hsu and J. Zhao, *Chemical Engineering Journal*, 2024, **484**.
8. L. Zhang, Y. Jin, G. H. Tao, Y. Gong, Y. Hu, L. He and W. Zhang, *Angew Chem Int Ed Engl*, 2020, **59**, 20846-20851.
9. L. Xie, Z. Zheng, Q. Lin, H. Zhou, X. Ji, J. L. Sessler and H. Wang, *Angew Chem Int Ed Engl*, 2022, **61**, e202113724.
10. C. Liu, W. Li, Y. Liu, H. Wang, B. Yu, Z. Bao and J. Jiang, *Chemical Engineering Journal*, 2022, **428**.
11. Z. Zheng, Q. Lin, L. Xie, X. Chen, H. Zhou, K. Lin, D. Zhang, X. Chi, J. L. Sessler and H. Wang, *Journal of Materials Chemistry A*, 2023, **11**, 13399-13408.
12. L. Thurakkal, S. R. Cheekatla and M. Porel, *Int J Mol Sci*, 2023, **24**.
13. A. Roja, S. Srividhya and M. Arunachalam, *Polymer*, 2024, **294**.
14. L. Zhang, Y. T. Luo, J. Q. Fan, S. J. Xiao, Q. Q. Zheng, X. L. Liu, Q. G. Tan, C. Sun, Q. Shi, R. P. Liang and J. D. Qiu, *J Hazard Mater*, 2024, **465**, 133488.
15. D. Dai, J. Yang, Y. C. Zou, J. R. Wu, L. L. Tan, Y. Wang, B. Li, T. Lu, B. Wang and Y. W. Yang, *Angewandte Chemie*, 2021, **133**, 9049-9057.
16. W. Y. Pei, J. Yang, H. Wu, W. Zhou, Y. W. Yang and J. F. Ma, *Chem Commun (Camb)*, 2020, **56**, 2491-2494.
17. Z.-Y. Zeng, Z.-C. Lou, L. Hu, W. Dou, X. Zhao, X. Li, J. Fang, X. Qian, H.-B. Yang and L. Xu, *Chemical Engineering Journal*, 2024, **496**.
18. M. Hao, Y. Xie, M. Lei, X. Liu, Z. Chen, H. Yang, G. I. N. Waterhouse, S. Ma and X. Wang, *J Am Chem Soc*, 2024, **146**, 1904-1913.
19. B. Tai, B. Li, L. He, Z. Ma, S. Lin, M. Zhang, J. Chen, F. Wu, L. Chen, X. Dai, F. Ma, Z. Chai and S. Wang, *Science China Chemistry*, 2024, **67**, 1569-1577.
20. W.-Z. She, Q.-L. Wen, H.-C. Zhang, J.-Z. Liu, R. S. Li, J. Ling and Q. Cao, *ACS Applied Nano Materials*, 2023, **6**, 18177-18187.

21. Y. Xie, T. Pan, Q. Lei, C. Chen, X. Dong, Y. Yuan, W. A. Maksoud, L. Zhao, L. Cavallo, I. Pinnau and Y. Han, *Nature Communications*, 2022, **13**.

22. L. He, L. Chen, X. Dong, S. Zhang, M. Zhang, X. Dai, X. Liu, P. Lin, K. Li, C. Chen, T. Pan, F. Ma, J. Chen, M. Yuan, Y. Zhang, L. Chen, R. Zhou, Y. Han, Z. Chai and S. Wang, *Chem*, 2021, **7**, 699-714.

23. X. He, S. Jia, B. Bao, Y. Li, E. Wang, L. Chen, H. Dan and Y. Ding, *J Hazard Mater*, 2024, **477**, 135413.

24. C. Balumuru, K. Raja, P. Sabharwall and V. Utgikar, *Nuclear Technology*, 2024, **210**, 1593-1601.

25. K. Jie, Y. Zhou, Q. Sun, B. Li, R. Zhao, D. E. Jiang, W. Guo, H. Chen, Z. Yang, F. Huang and S. Dai, *Nat Commun*, 2020, **11**, 1086.

26. B. Li, X. Dong, H. Wang, D. Ma, K. Tan, S. Jensen, B. J. Deibert, J. Butler, J. Cure, Z. Shi, T. Thonhauser, Y. J. Chabal, Y. Han and J. Li, *Nat Commun*, 2017, **8**, 485.

27. X. Gao, Q.-H. Hu, Y.-Z. Shi, R.-P. Liang and J.-D. Qiu, *Separation and Purification Technology*, 2025, **359**.

28. C. Tan, L. Jiang, R. Xiong, H. Wang, C. Yan, R. Wang, C. Liu, Y. Liu, X. Dai, T. Duan, W. Liu and L. Zhu, *Inorg Chem*, 2024, **63**, 23877-23885.

29. T. Pan, X. Dong and Y. Han, *Nano Research*, 2023, **16**, 6308-6315.

30. N. Arora, T. Debnath, M. C. Senarathna, R. M. Johnson, I. G. Roske, G. A. Cisneros and R. A. Smaldone, *Chem Sci*, 2024, **15**, 3571-3577.

31. D. Chen, T. Ma, X. Zhao, X. Jing, R. Zhao and G. Zhu, *ACS Appl Mater Interfaces*, 2022, **14**, 47126-47135.

32. P. Mao, B. Qi, Y. Liu, L. Zhao, Y. Jiao, Y. Zhang, Z. Jiang, Q. Li, J. Wang, S. Chen and Y. Yang, *Journal of Solid State Chemistry*, 2016, **237**, 274-283.

33. R. Liu, W. Zhang, Y. Chen, C. Xu, G. Hu and Z. Han, *Separation and Purification Technology*, 2020, **233**.

34. D. K. L. Harijan, V. Chandra, T. Yoon and K. S. Kim, *J Hazard Mater*, 2018, **344**, 576-584.

35. Y. Yin, Y. Yang, G. Liu, H. Chen, D. Gong, Y. Ying, J. Fan, S. Liu, Z. Li, C. Wang, Z. Guo, Z. Li, C. Yu and G. Zeng, *Chemical Engineering Journal*, 2022, **441**.

36. H. J. Choi and M. P. Suh, *Journal of the American Chemical Society*, 2004, **126**, 15844-15851.

37. T. He, X. Xu, B. Ni, H. Lin, C. Li, W. Hu and X. Wang, *Angew Chem Int Ed Engl*, 2018, **57**, 10148-10152.

38. R. Gao, B. An, C. Zhou and X. Zhang, *Molecules*, 2022, **27**.

39. H. Li, Y. Li, B. Li, D. Liu and Y. Zhou, *Chemosphere*, 2020, **252**, 126448.

40. L. Hashemi and A. Morsali, *CrystEngComm*, 2012, **14**, 779-781.

41. A.-N. Au-Duong and C.-K. Lee, *Crystal Growth & Design*, 2018, **18**, 356-363.

42. Z. Wang, Y. Huang, J. Yang, Y. Li, Q. Zhuang and J. Gu, *Dalton*

transactions, 2017, **46**, 7412-7420.

43. L. Hashemi and A. Morsali, *CrystEngComm*, 2014, **16**, 4955-4958.

44. S.-Q. Xu, T.-G. Zhan, Q. Wen, Z.-F. Pang and X. Zhao, *ACS Macro Letters*, 2016, **5**, 99-102.

45. Q. Tao, L. Sun and L. Jing, *Separation and Purification Technology*, 2025, **353**.

46. Y. Ju, Z.-J. Li, J. Qiu, X. Li, J. Yang, Z.-H. Zhang, M.-Y. He, J.-Q. Wang and J. Lin, *Inorganic Chemistry*, 2023, **62**, 8158-8165.

47. Y. Liao, J. Li and A. Thomas, *ACS macro letters*, 2017, **6**, 1444-1450.

48. X. He, L. Chen, X. Xiao, Y. Gan, J. Yu, J. Luo, H. Dan, Y. Wang, Y. Ding and T. Duan, *Chemical Engineering Journal*, 2023, **462**.

49. L. Jiang, Z. Yin, J. Chu, C. Song and A. Kong, *Journal of Solid State Chemistry*, 2022, **306**.

50. Q. Tao, X. Zhang, L. Jing, L. Sun and P. Dang, *Molecules*, 2023, **28**.

51. J.-Y. Xian, Z.-Y. Huang, X.-X. Xie, C.-J. Lin, X.-J. Zhang, H.-Y. Song and S.-R. Zheng, *Chinese Journal of Structural Chemistry*, 2023, **42**.

52. S. Xu, J. Ma, H. Jia, M. Zhang, Y. Qu, C. Geng, X. Zhao, M. Shao, J. Xu and X. Wang, *Int J Biol Macromol*, 2025, **294**, 139412.

53. H. Fu, Y. Tang, Q. Yuan, J. Chang, F. Liao, J. Zhang, H. Gao, Y. Yang and Y. Liao, *Fuel*, 2024, **371**.